ACES Asian Chemical Editorial Society

doi.org/10.1002/cnma.202300275

CHEMNANOMAT
Research Article

www.chemnanomat.org

Low-cost Photoactive Hybrid Materials: From Green Synthesis to Multi-technique Analytical Characterization

Eleonora Conterosito,[a] Valentina Toson,[b] Enrico Boccaleri,[a] Diego Antonioli,[b] Marco Milanesio,[b] Luca Palin,[b, c] Claudia Barolo,[d, e, f] Nadia Barbero,[d, e] Simone Galliano,[d] and Valentina Gianotti*[a]

Abstract: Low-cost photoactive hybrid materials for light management, based on neutral organic molecules intercalated into saponite, were prepared by facile green methods and characterized. TPBI (2-(2'-tosylaminophenyl)benzimidazole) was chosen as an organic host dye, envisioning its application as a downconverter in silicon or dye-sensitized photovoltaic modules. Mixed with a cationic surfactant, the neutral molecule was intercalated with a sort of "trojan horse" approach by an easy, almost solvent-free method, thus limiting its aggregation. The obtained material was characterized by combining spectroscopic, diffractometric, and microscopic techniques. Moreover, the intercalation of the dye, the species present in the interlayer, their stability and mutual interactions were assessed by TGA-GC-MS. We obtained a material containing a fluorescent dye in the solid state and stabilized by intercalation and dispersion into saponite. At last, this material was used to prepare a photoactive polymer by melt blending, obtaining materials with the desired optical properties, with Stokes shifts larger than 100 nm and an emission yield above 50%.

Introduction

Light management[1] is intended as tuning an incoming radiation (ranging from the UV to the IR range) to improve the efficiency and stability of a device when illuminated by a natural or artificial source. In the specific case of photovoltaics (PV), it is intended to maximize the photovoltaic solar energy conversion by modifying the features of the PV device.[2] The model is the vegetal world, where chlorophyll is assisted by the ancillary dyes present in the leaves to enhance the light conversion during photosynthesis and protect the leaves from degradation.

The enhancement of the light-harvesting efficiency both in PV silicon modules and in Dye-Sensitized Solar Cells (DSSC) is pursued by using photoactive materials able to absorb at specific wavelengths and emit in another region at a lower or higher frequency in the region where the PV module is more efficient.[3] Different materials such as ZnO doped with rare earth elements, d-block complexes, quantum dots and organic/metallorganic dyes are being studied.[4–8]

The main advantages of organic fluorophores with respect to other materials are the improved luminescence, quantum efficiency, a wide range of colors, lower cost, and easy synthesis. Drawbacks are higher re-adsorption issues and usually a lower UV stability within time. To address these issues, in this study, the down-conversion[9] of the solar UV fraction (not helpful and also harmful for Si-based PV cells) to the visible region was pursued by exploiting a photoactive organic molecule stabilized by intercalation in an inorganic host. This possibility was suggested by the notorious ancient hybrid pigments such as Maya Blue,[10] where outstanding stability and resistance of an organic pigment is achieved by its incorporation in an inorganic matrix. Moreover, the dispersion between the surfactant molecules helps prevent aggregation of the fluorophore molecules, which reduces their fluorescence, increasing quantum efficiency. This approach, characterized by easy tunability,

[a] Dr. E. Conterosito, Prof. E. Boccaleri, Prof. V. Gianotti
DiSSTE – Dipartimento per lo Sviluppo Sostenibile e la Transizione Ecologica
Università del Piemonte Orientale
Piazza S. Eusebio 5, 13100 Vercelli (VC) (Italia)
E-mail: valentina.gianotti@uniupo.it

[b] Dr. V. Toson, Dr. D. Antonioli, Prof. M. Milanesio, Dr. L. Palin
DiSIT – Dipartimento di Scienze e Innovazione Tecnologica
Università del Piemonte Orientale
Viale T. Michel 11, Alessandria 15121 (AL) (Italia)

[c] Dr. L. Palin
Nova Res s.r.l., Via D. Bello 3, 28100 Novara, Italy

[d] Prof. C. Barolo, Prof. N. Barbero, Dr. S. Galliano
Dipartimento di Chimica, Centro Interdipartimentale NIS, Centro di Riferimento INSTM
Università di Torino
Via G. Quarello 15a, 10135 Torino (TO) (Italia)

[e] Prof. C. Barolo, Prof. N. Barbero
Istituto di Scienza, Tecnologia e Sostenibilità per lo Sviluppo dei Materiali Ceramici (ISSMC-CNR)
Via Granarolo 64, 48018 Faenza (RA) (Italia)

[f] Prof. C. Barolo
Centro Interdipartimentale di Innovazione ICxT
Università di Torino
Lungo Dora Siena 100, 10153 Torino (TO) (Italia)

Supporting information for this article is available on the WWW under https://doi.org/10.1002/cnma.202300275

could also be exploited for the preparation of a co-absorber to be used in DSSCs by changing the photoactive molecule and/or host.[11–13] The prepared hybrid material is then used as additive in the polymeric film covering the PV cell. The suitability of the material as additive in polymers is widely reported in the literature where similar clays are successfully exploited, e.g. for improving the fire resistance and gas barrier properties of the polymers.[14–19] Regarding the preparation of the hybrid, based on the experience from our previous works using a quasi-solid state approach to intercalate chromophore molecules into layered double hydroxides (LDH), which can host anionic species,[20] we were able to extend the possibility to the use of cationic and neutral dyes by changing the host.[21,22] In this work we have developed the intercalation method, testing its applicability with a different and more complex molecule, this time chosen specifically to produce a material with a real world application. Moreover, here the material was included in a polymer and the obtained films were studied. The advantages of the intercalation method here exploited, called Liquid Assisted Grinding (LAG), are the limited use of solvent and the rapidity of the intercalation (seconds/minutes) with respect to conventional methods, such as the hydrothermal method or ionic exchange, requiring several hours under stirring and heating and a large amount of solvent.[23]

Saponite was selected as host material, as an alternative to LDH, for the wider possibility of tuning its size, specific surface area and porosity by choosing the appropriate synthetic conditions. Saponite is also easily delaminated and has a high exchange capacity; it can be found in nature or synthesized.[24] Furthermore, with respect to LDH, which has higher crystallinity, saponite is delaminated more easily, forming thinner bunches of layers.

Saponite is a trioctahedral 2:1 clay mineral belonging to the smectite group;[25] it has a layered structure based on two tetrahedral aluminosilicate layers (T), with an octahedral layer based on di/trivalent hexa-coordinated ions (O) in between. The general formula of saponite is $M^{n+}_{x/n}[Mg]_6(OH)_4[Si_{8-x}Al_x]O_{20}\cdot mH_2O$, where M are the exchangeable cations of charge *n*, residing in the interlayer space, *x* is the fraction of aluminum contained in the T structure and *m* is the number of water molecules. In square brackets are the cations composing the O sheet. The isomorphous substitution of Si with Al in the T sheet generates a negative charge that can vary between 0.2 and 0.6 units of charge for half unit cell. This negative charge can be compensated by counter-ions bearing a positive charge, like alkaline and alkaline earth ions localized in the interlayer spaces. The total amount of intercalated cations is the cation exchange capacity (CEC), and it is expressed as milliequivalents of cations for 100 g of clay. The interlayer space has a variable thickness depending on both the charge of the lamellae and on the cationic species hosted in this region.

After a literature survey on fluorophores structures, thanks to its interesting optical properties and easy synthesis, the 2-(2′-tosylaminophenyl)benzimidazole (TPBI) molecule was chosen[26,27] (see structure in Figure 1). TPBI is a neutral molecule, presenting a significant Stokes shift (i.e. the shift between the maxima of the peak of absorption and emission

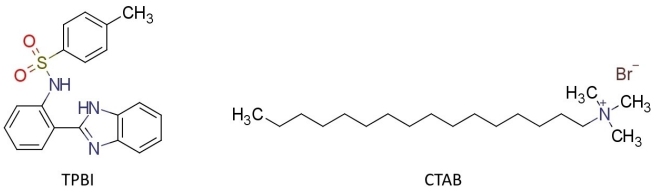

Figure 1. Chemical structures of TPBI and CTAB, used as guests for intercalation into saponite.

for an electronic transition, in this case the absorption falls in the UV region and the emission is in the visible range), of about 155–180 nm (depending on solvent) combined with a remarkable quantum yield, about 59% (in dichloromethane).[28,29]

The intercalated sample, namely *CTA_TPBI_Sap*_LAG, was obtained by LAG exchange[20,21,30] starting from an inorganic saponite, and it was fully characterized through the combination of spectroscopic, diffractometric and microscopic analysis. The intercalation of the emitter in the interlayer space of saponite is expected to improve its durability, stability, and dispersion.

A qualitative assessment of the presence of the dye was obtained by spectroscopic techniques such as FT-Raman, FT-IR and diffuse reflectance coupled with fluorescence analysis but not the definitive confirmation of the intercalation within the layers. Here we were able to distinguish, following an approach tested in a previous work[21] the intercalated species from the adsorbed ones exploiting TGA-GC-MS.

TGA-GC-MS analyses[31,32] were performed because this technique has proved helpful in many cases for the characterization of organo-modified anionic layered samples[10,33] and saponite[21] and provides information about the strength of the interactions between the inorganic skeleton of saponite and the organic molecules through the analysis of the thermal behavior of the organic molecules. Moreover, we were able to quantify the hosts species by coupling the information obtained by TGA with CHN analysis and XRF analysis.

This material was finally employed and tested by melt blending in a polymer to obtain a new photoactive polymer which was fully characterized.

Results and Discussion

Saponite (*Na-Sap110*) was prepared as detailed in the experimental section. An amount of this sample was used as a host material for the dye, while some was kept as reference material for the analysis. Here a Si/H_2O ratio equal to 110 was chosen[34] for the synthesis, as from a preliminary feasibility study carried on with a neutral molecule available in large amounts and at low cost, i.e. fluorene, successful intercalation was obtained,[21] thanks to the co-intercalation of cetyltrimethylammonium bromide (CTAB), a cationic surfactant. The neutral dye is expected to interact and stay between the long hydrophobic chains of the surfactant and be carried by the surfactant inside the saponite.

TPBI was intercalated into *Na-Sap110* exploiting liquid-assisted grinding (LAG), which consists in grinding in a mortar saponite and the desired guest molecule in the presence of a limited amount of solvent. To achieve the intercalation of the dye, which is neutral, a solution of TPBI with the surfactant (CTAB) was prepared beforehand, as detailed in the experimental section. The obtained material, the *CTA_TPBI_Sap* sample, was studied from the structural, compositional, and morphological point of view, and then its optical features and thermal stability were evaluated. Finally, the material was employed in a real application as an additive in an acrylic block copolymer suitable for PV applications. Compounding tests were performed by melt blending using a Kurarity polymer, exploiting its high transparency and UV light resistance. Four kinds of the film were prepared for comparison:

i) film without any additive (*Kurarity*)
ii) film with only inorganic saponite as additive (*Kur_NaSap110*)
iii) film with the intercalated material (*Kur_CTA_TPBI_Sap*)
iv) film obtained dispersing directly the dye in the polymer (*Kur_TPBI*)

The amounts of *CTA_TPBI_Sap*, saponite and TPBI added in the polymer are reported in Table 1 and are expressed as PHR (grams of additive per 100 g of polymer). The reported values were chosen after preliminary tests to keep good transparency of the film and adequate optical density. The amount of TPBI directly dispersed in the Kurarity polymer was chosen after the determination of the amount of intercalated TPBI in the *CTA_TPBI_Sap* sample to be similar or higher.

Such tests also allowed calibrating the extruder, finding the best temperature, residence time and speed of the screws during circulation and extrusion, which are reported in the experimental section. At last, the polymeric films were analyzed by microscopy and their performances were evaluated by spectroscopic characterization and compared.

Assesment of intercalation

X-ray powder diffraction

XRPD analysis was carried on the inorganic saponite and on the intercalated sample to obtain the immediate assessment of the success of intercalation by the evaluation of the interlayer spacing. In Figure S1 the XRPD patterns of *Na-Sap110* and *CTA_TPBI_Sap* are reported. The basal peak, related to the order perpendicular to the layers, is sharper in the *CTA_TPBI_Sap* sample, evidencing that the presence of the surfactant makes the interlayer distance more regular. The increase of the interlayer distance, shown by the shift of the basal peak (001) from 7.9° 2θ (11.2 Å) for *Na_Sap110* (grey curve) to 6.2° (14.2 Å) for the intercalated sample is a sign of the success of the intercalation. This interlayer distance agrees with the intercalation of the surfactant with its chains parallel to the layers. Attempts were made using surfactants with different chain lengths and different amounts of surfactant to obtain the intercalation with the chains perpendicular to the layers, but the d-spacing were always similar, indicating that the intercalation always occurred with the surfactant lying almost flat between the layers. The XRPD pattern of the sample intercalated with CTAB without TPBI was also included for comparison. The increase in the d-spacing is not different when CTA^+ is intercalated alone or with TPBI. In fact, TPBI sits in between the alkyl chains of the surfactant without causing a further increase of the interlayer distance. The absence of peaks attributable to crystalline CTAB or TPBI indicate that eventual residues of guest molecules were successfully removed by washing.

SEM/EDX analysis

The SEM image of the *CTA_TPBI_Sap* sample, reported in Figure S2, confirms that the sample mantains the characteristic layered morphology of saponite. Thin, non-flat sheets of about (10 nm) thickness are grouped in large aggregates with a size of several microns.

The EDX analysis was performed by dripping the compound over a polymer film to avoid interferences from the Al stub or the adhesive tape (containing sulfur) and sampling was performed in five different points (see Table S1). The stoichiometric ratios of elemental components of saponite agree with the expected saponite composition for all the points.

FT-Raman and FT-IR analysis

FT-Raman spectra of the dye alone (*TPBI*) and of the intercalated sample (*CTA_TPBI_Sap*) are reported in Figure 2. In Figure 2 the spectra of solid state TPBI and of the intercalated sample show that TPBI has many Raman active vibrations while *CTA_TPBI_Sap* spectrum shows a few bands only and a high background signal, probably due to the low crystallinity of the saponite matrix and to fluorescence. However, the presence of of TPBI in the sample is confirmed by the presence of its characteristic

Table 1. Amounts of polymer and additives for the extrusion.

Film sample name	Polymer (g)	Additive (g)	Additive name	PHR[a]
Kurarity	*5.00*	–	–	–
Kur_NaSap110	*4.00*	0.058	*NaSap110*	1.45
Kur_TPBI	4.00	0.006	*TPBI*	0.15
Kur_CTA_TPBI_Sap	4.00	0.064	*CTA_TPBI_Sap*	1.60

[a] Grams of additive per 100.00 g of polymer.

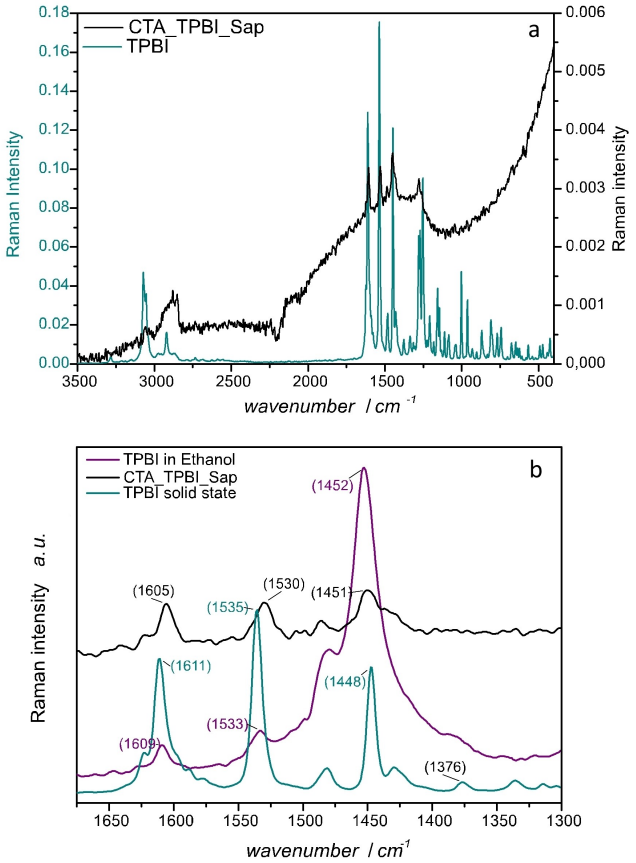

Figure 2. FT-Raman spectra from 3500 to 400 cm^{-1} (a) and detail of the spectral range from 1675 to 1300 cm^{-1} (b).

signals. In particular, the C–H stretching bands of aromatics at about 3000 cm^{-1} and the relative bending mode at around 1600 cm^{-1}; the C–H stretching of isolated methylene that falls at 2920 cm^{-1}, and the C–H bending at 1375 cm^{-1}. The N–H stretching of the secondary amine of sulfonamide groups is Figure 2.

Centered at 3279 cm^{-1}, while the C–N stretching falls around 1200–1130 cm^{-1}. The band due to S=O asymmetric stretching of the sulfonamide group is weak and therefore visible only in the pure TPBI spectrum at 1335 cm^{-1} together with a sharp band at 1156 cm^{-1} for the symmetric stretching. The aliphatic CH str. in the 2800–3000 cm^{-1}, visible in the intercalated sample (*CTA_TPBI_Sap*), are attributable to the CTA chains. Regarding the saponite matrix, according to the literature, the structural modes υ1 and υ5 of SiO_4 tetrahedra at 678 and 360 cm^{-1} are not active for saponite with H_2O/Si ratio equal to 110 and therefore are not visible in the *CTA_TPBI_Sap* spectrum.[34]

A detail of the 1675–1300 cm^{-1} range of the intercalated sample is shown in Figure 2b, together with the spectra of TPBI in ethanol (the solvent used for LAG) for comparison. The TPBI modes in *CTA_TPBI_Sap* are shifted at lower cm^{-1} with respect to the pure dye in the solid state indicating that the arrangement of TPBI and its chemical environment in the intercalated material is indeed different from that of the pure dye in the solid state. The same shift is present, even if less accentuated, in the spectrum collected in ethanol solution.

The arrangement of the surfactant and dye after intercalation is further confirmed by FT-IR spectroscopy, not affected by sample fluorescence. The FT-IR spectra of the sample are shown in Figure 3. The typical bands of both *Na-Sap110* and TPBI are present in the *CTA_TPBI_Sap* sample. The bands of the asymmetric and symmetric S=O stretching are here visible also in the spectra of the intercalated compound and shifted at different wavenumbers with respect to the spectra of the dye alone (the asymmetric stretching from 1335 to 1339 cm^{-1} and the symmetric stretching from 1156 to 1163 cm^{-1}) confirming once again that the dye environment is different and therefore the intercalation procedure was effective. The band falling at 3287 cm^{-1} in the TPBI spectra is ascribed to the NH stretching but is no longer visible in the intercalated sample because it is broadened by the formation of different kinds of hydrogen bonds. The CH stretching bands of CTAB falling in the 3000–2850 cm^{-1} region are also clearly visible in the *CTA_TPBI_Sap* sample and almost unaffected by the intercalation.

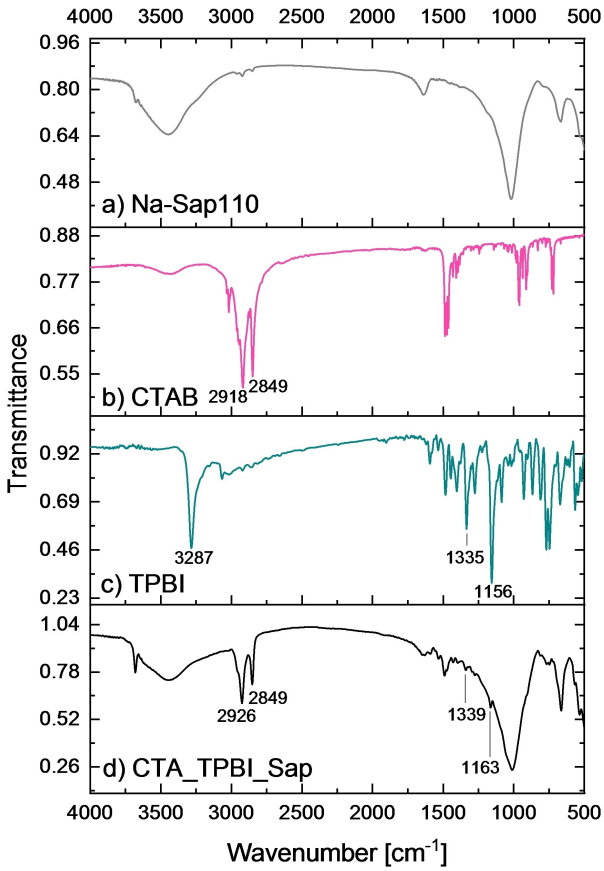

Figure 3. FT-IR spectra from 4000–400 cm^{-1} of *Na-Sap110* (a), CTAB (b), TPBI (c), and the intercalated sample *CTA_TPBI_Sap* (d).

Thermal analysis

The thermal behavior of *CTA_TPBI_Sap* and TPBI was studied by thermogravimetric analysis (TGA) to estimate the organic fraction in the sample. The sample and dye degradation profiles are reported in Figure S3 as TG and dTG profiles.

The %weight losses of the intercalated sample were compared to those of the inorganic *Na-Sap110* and of the pure TPBI dye (Figure S3). The total weight loss in the intercalated sample resulted in 36.5% and is due to loss of water, dehydroxylation and loss of the organic fraction.

As previously reported,[21] we observed that the organo-modification of saponite with CTA^+ changes the hydrophilic behavior of the saponite interlayer, in fact, in the present case, the physi-chemisorbed water in the intercalated sample is only 1% with respect to 7% in the *Na-Sap110* samples. From the total thermogravimetric loss, excluding water and dehydroxylation, the quantity of organic in *CTA_TPBI_Sap* can be estimated around 32–33%.

The most evident weight loss, due to the organic fraction of the *CTA_TPBI_Sap* sample occurs in two broad steps between 200 and 300 °C and between 325 and 450 °C (Figure S3). By comparison with the reference thermal profiles of the surfactant and of the dye, the first weight loss can be ascribed to the surfactant and the second one to the dye. A broad weight loss is then present over 600 °C, indicating the occurrence of chemical transformations involving the dye. In fact, the TG profile of TPBI alone shows a similar weight loss.

To further investigate on the nature of the weight losses TGA-GC-MS analyses were carried out since the evolved gases from TGA at each temperature can be separated and identified.

The analyses were performed at the same heating rate and flow used for the TGA analysis, i.e. 10 °C/min (Figure 4) on the pure TPBI and CTAB and on the *CTA_TPBI_Sap* sample.

As can be seen from Figure 4, the gas evolved during TGA consists of many different fragments and its composition changes with the temperature. The identity and origin of all fragments evolved from the intercalated sample was deter-

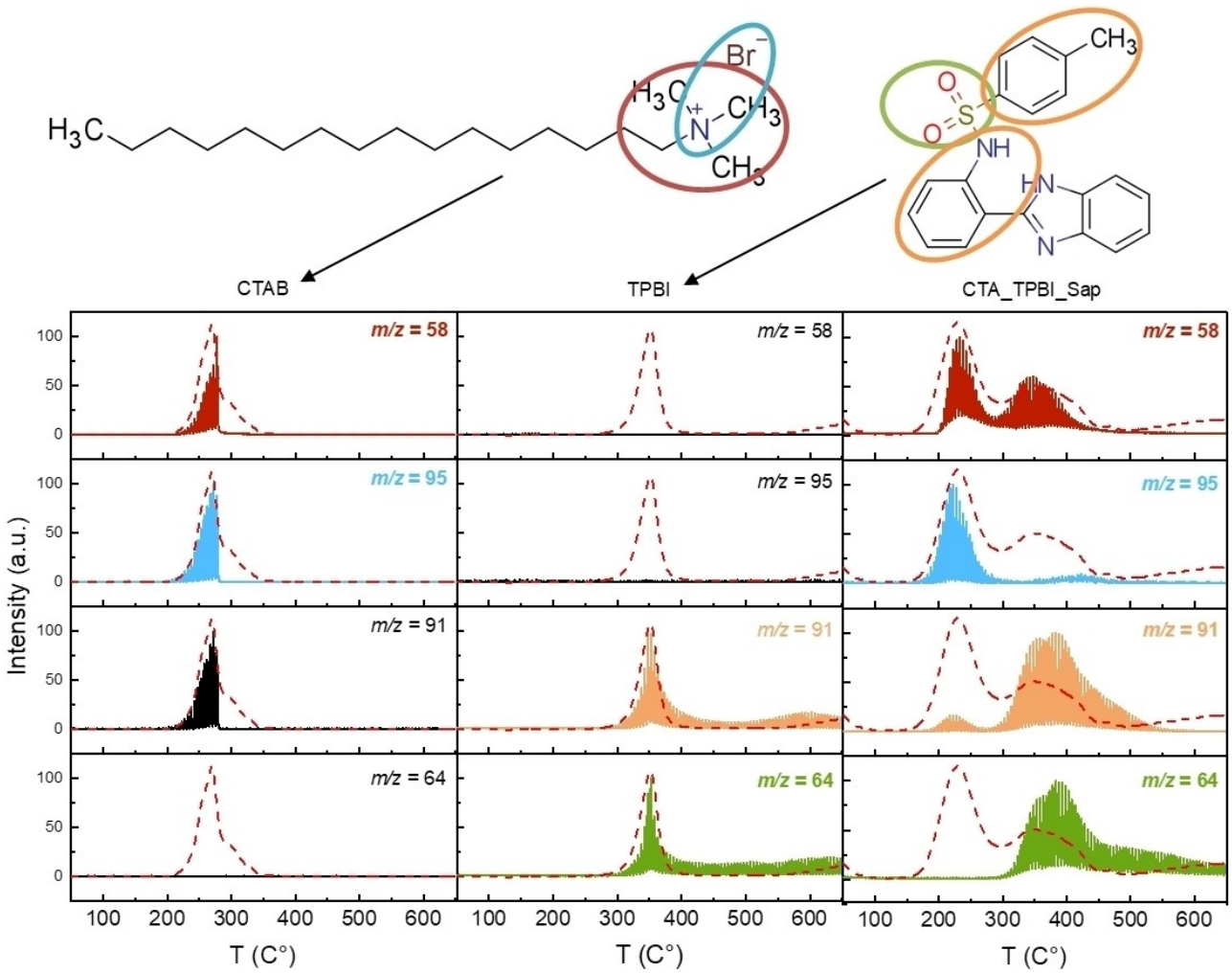

Figure 4. TG-GC-MS curves associated to fragments m/z 58 and 95 for CTAB, to fragments 91and 64 m/z for TPBI and to all four fragments for the intercalated sample CTA_TPBI_Sap, recorded under inert flow at 5 °C/min.

mined by comparison with the analysis of the individual components throughout the thermal program.

The m/z signals at 95 and 58 are characteristic of CTAB (Figure 4) which shows a single weight loss centered between 200 and 250 °C, as reported in literature.[21] The fragment at 58 m/z can be assigned to the residue $[N(CH_3)_3]^+$, charged and without bromine as a counter-ion. The 95 m/z corresponds instead to the same fragment but dealkylated and forming an adduct with Br^-. The same signals extracted from the analysis of the *CTA_TPBI_Sap* sample (Figure 4 right panel) show two different behaviors. In fact, the 58 m/z fragment profile shows the presence of two distinct weight losses: the first one centered between 200 and 250 °C, which can be ascribed to CTA^+ adsorbed on the surface of saponite (since it occurs at the same temperature in the pure CTAB sample) and the second one, broader and centered at 350 °C, indicating that part of the CTA^+ evolves at higher temperatures with respect to the pure CTAB, which can be ascribed to CTAB intercalated inside the layers.

The fragment at 95 m/z shows instead only one peak of evolution centered at low temperatures, meaning that the part of CTAB salified with the Br^- is weakly bound so it can be inferred that it is not stabilized by intercalation and therefore remains only on the surface. Therefore, CTAB is adsorbed only on the surface and not intercalated while CTA^+ is in part intercalated (and stabilized thermally) and in part outside the layers (and therefore evolved at lower temperatures).

A separate investigation must be made for the profile of the fragment at m/z 91 because it is attributable to both the CTAB and the TPBI. In CTAB, the peak at m/z 91 is centred at 250 °C, while in TPBI is centered around 350 °C. In the intercalated sample the profile of this signal has two peaks; the less intense one falls at lower temperatures, between 200 and 250 °C, at the same temperature where other fragments attributed to non-stabilized CTA^+/CTAB fall.

The main loss is placed around 300–530 °C and it does not seem completely resolved since two contributions can be identified. To better resolve the co-elution, analyses were replicated with 5 °C/min and 20 °C/min heating ramps (Figure S4). Anyway, changing the ramp speed did not highlight any significant variation in the thermal processes. It can be hypothesized that the peak part around 350 °C is due to CTAB while the part at higher temperatures is attributable to TPBI. Both species are stabilized by the intercalation.

This hypothesis is confirmed by observing the other typical fragment of the TPBI, the 64 m/z. It is more informative of the fate of the TPBI when interspersed because it is not present in any other component and is very characteristic since it corresponds to the portion containing sulfur (SO_2). In fact, such fragment shows a peak in the intercalated sample positioned exactly around 390 °C.

CEC value, XRF and Elemental Analysis

The CEC value, determined by the cobalthexamine ion ($[Co(NH_3)_6]^{3-}$) method (CoHex method),[18,26,27] resulted to be 50.94 meq/100 g. Since 69.4 wt.% of the sample is inorganic (i.e. saponite), the amount of CTA^+ to be intercalated to counter-balance the positive charges of saponite is $3.535*10^{-04}$ mol in each gram of sample, corresponding to about 10% wt of CTA^+ in the sample.

An XRF analysis was performed on the intercalated sample. In particular, the amount of sulfur and bromine was measured since sulfur is only present in TPBI and bromine only in CTAB, allowing their quantification. The measurements were validated by a calibration performed with different mixtures of saponite, TPBI and CTAB. The amount of neutral CTAB, absorbed on the surface, (see Table S2) resulted of the 11 wt.% while the amount of TPBI resulted 6 wt.%

Assuming the intercalation of CTA^+ to be complete, its percentage in weight can be calculated from the CEC to be 10 wt.%. These results indicate a total amount of organic in the sample of 27 wt.%.

These calculations are supported by CHN analysis performed on the *CTA_TPBI_Sap* sample (Table S4) and on a saponite prepared using the same method to intercalate CTAB without adding the TPBI dye (*CTA_Sap*, see Table S3). Assuming the amount of CTA/CTAB intercalated to be dependent from the number of charges in the layers only, and not influenced by the co-intercalation of TPBI, the differences in the %C and %N between the two samples can be ascribed to TPBI only (see Table S3 and S4). The amount of TPBI resulted therefore about 7 wt.%. The remaining %C is due to CTAB and CTA^+. These results are in good agreement with the TGA and XRF analysis. Overall, the total percentage of organic (31 wt.%) measured by CHN analysis confirms the TGA results. The weight ratio between CTAB and TPBI used for the synthesis (reported in the Experimental section) appears to be maintained inside saponite.

Spectroscopic characterization of the intercalated saponites

A thorough UV–Vis spectroscopic characterization was carried out both on the sample alone and applied in a real-world situation (as additive in a polymer film) to assess its performances and compare it to those of the pure dye.

From the DR-UV reflectance spectrum of *CTA_TPBI_Sap* reported in Figure 5, two main maxima at 260 nm and 358 nm can be highlighted together with a less defined and wide absorption band placed around 280–340 nm. The corresponding Na-Sap110 spectrum (Figure S5) shows only a very weak and broad absorption band at about 270 nm.

Based on the absorption spectra, a photophysical characterization was performed recording the emission spectra from 400 to 550 nm while irradiating in correspondence of the two absorption maxima at $\lambda = 260$ and 358 nm (Figure 5b). The excitation at 260 nm causes an emission centered at 468 nm (purple line in Figure 5b) reaching an intensity of about $2*10^5$ CPS, while the 358 nm excitation promotes an emission four times more intense (black line) and centered at 466 nm, with a Stokes shift (as the difference between the maximum of emission (466 nm) and the excitation wavelength (358 nm)) of 108 nm. This value is 29 nm lower than that of the dye disperse

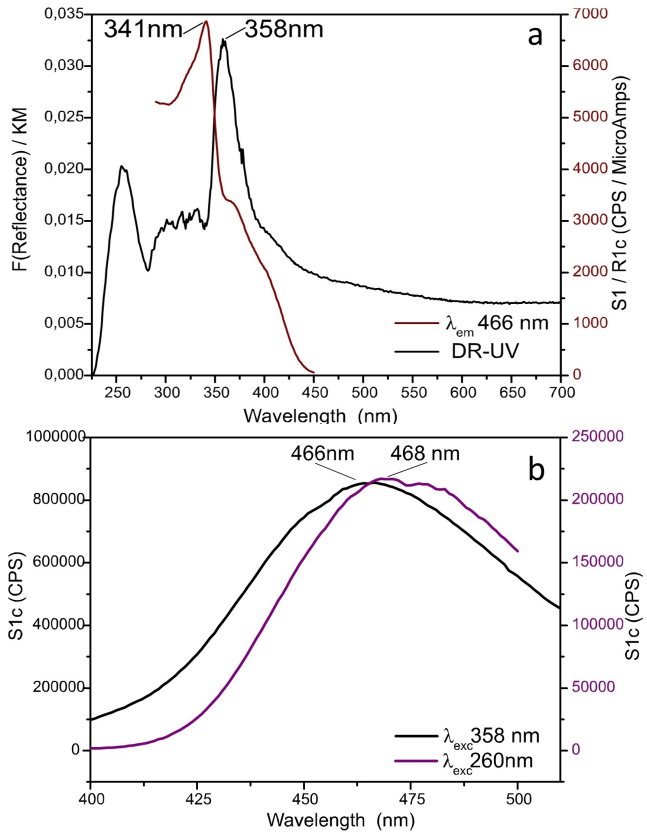

Figure 5. (a) DR-UV/Vis spectrum of *CTA_TPBI_Sap* recorded from 200–700 nm in $BaSO_4$ (black line). FL excitation spectrum of *CTA_TPBI_Sap* at λ 466 nm, recorded from 290–450 nm (dark red line) with 2 nm and 2 nm aperture slits and 2 seconds of integration time. (b) Emission spectra of *CTA_TPBI_Sap* recorded at λ 260 nm (purple) and λ 358 nm (black) with 2.5 nm and 3 nm aperture slits and 2 seconds of integration time. The scale on the y axis on the left is referred to the spectrum recorded with excitation at 358 nm and the scale on the right to the excitation at 260 nm.

in acidic water (Figure S6). The most relevant contribution to the emission at 466 nm can be evaluated from the fluorescence excitation spectrum. This spectrum (purple line in Figure 5a) was recorded scanning the absorption in the 290–450 nm range with the emission wavelength fixed at 466 nm, and reveals that the emission at 466 nm is mostly due to the absorption at 358 nm; hence, the Stokes shift was calculated between these two wavelengths and resulted of 125 nm, a good result for a nanocomposite material, ready to be dispersed into a polymer.

Characterization of polymer films

The sample *CTA_TPBI_Sap* and *TPBI* alone were dispersed in the Kurarity polymer and filmed as described in the experimental section. To assess if the dispersion of the additives in the film is satisfactory a preliminary analysis of the four film samples, detailed in Table 1, was carried out by optical and SEM microscopy and irradiating with an UV-lamp (see Figure S7) to assess the homogeneity of the dispersion of the additives in the polymer. SEM images were collected on the *Kur_CTA_TPBI_Sap* and are reported in Figure S8 together with the EDX maps for Silicon, Magnesium and Aluminum which helped to distinguish the saponite particles into the Kurarity film.

Saponite dispersion was also evaluated via image analysis (Figure S9) of the film surface to estimate the % of the surface covered by saponite particles, which resulted of about 6%.

Spectroscopic characterization of polymer films

ATR FT-IR spectra were collected from 4000 to 400 cm^{-1} on the films, but the IR absorption modes of the additives are not observed (see Figure S10), since the amount of additive is too low for the sensitivity of such technique.

The UV–Vis absorption profiles of *Kurarity*, *Kur_NaSap110*, *Kur_CTA_TPBI_Sap* and *Kur_TPBI* films are shown in Figure 6. The Kurarity and NaSap110 absorptions are low, and they are irrelevant for the optical features of the films. The *Kur_TPBI* and *Kur_CTA_TPBI_Sap* (see Figure 6) spectra show some differences due to the intercalation in the inorganic matrix. Despite the similar amount of TPBI in the two formulations (the amount of TPBI directly dispersed into the polymer is 9% wt. with respect to the amount of *CTA_TPBI_Sap*, while the amount of TPBI intercalated into the *CTA_TPBI_Sap*, resulting from the quantitative measurements is around 6–7 wt.%.), in the case of *Kur_CTA_TPBI_Sap* the relative intensities of the absorption features are in general higher and, basically, with different intensity ratio, suggesting that the chromophore's features are enhanced by intercalation but the absorption occurs at the same wavelength in both samples. Conversely, when analyzing the *CTA_TPBI_Sap* before and after the compounding into the polymer (Figure 7), it can be seen that this procedure causes a little blue shift of the UV absorption of the dye from 358 nm to about 260–335 nm, modifying the absorption profile of TPBI in shape and spectral positions (see Figure 7).

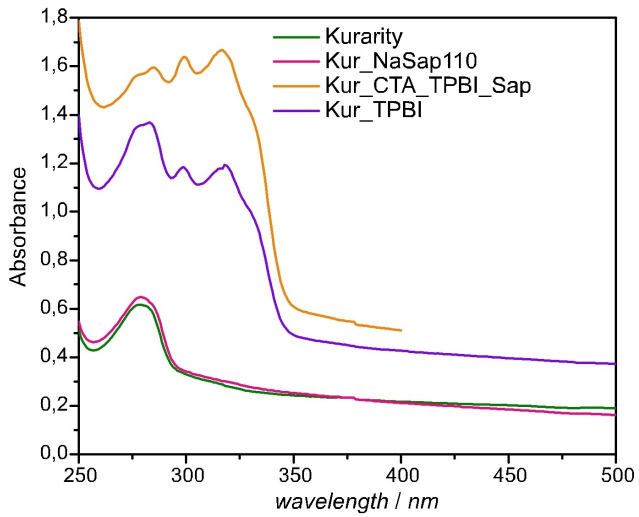

Figure 6. UV–Vis spectra in transmission of *Kurarity* (olive), *Kur_NaSap110* (pink), *Kur_CTA_TPBI_Sap* (orange) and *Kur_TPBI* (violet) films 100 μm.

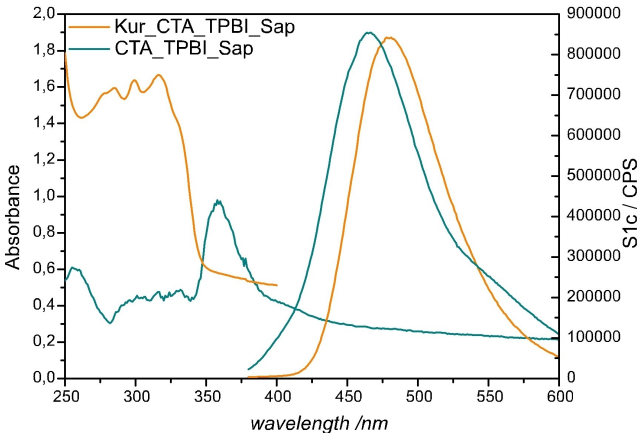

Figure 7. Absorption (left) and emission (right) spectra of *CTA_TPBI_Sap* (dark cyan) and *Kur_CTA_TPBI_Sap* (orange). Sample *CTA_TPBI_Sap* absorption spectrum is converted in absorbance units from the relative Dr-UV spectrum.

The emission spectra of the *Kur_CTA_TPBI_Sap* sample, reported in Figure S11, were recorded exciting at $\lambda = 300$ nm, 310 nm, 316 nm, 320 nm, keeping the same experimental conditions. All spectra show the emission maximum at 481 nm, and the excitation at 320 nm gives the most intense emission, therefore the Stokes shift is 161 nm. Hence, the Stokes Shift increases with the dispersion of the *CTA_TPBI_Sap* sample into the Kurarity polymer of 53 nm (Figure 7). Furthermore, the fluorescence excitation spectrum was measured with emission wavelength fixed at 481 nm (Figure 8), showing that, between the absorption at 333 nm and the one at 320 nm, the former represents the main contribution to the emission, providing a Stokes shift equal to 148 nm. To favor the comparison of the Stokes shift values, considering the dispersion of the dye in the interlayers of the clay similar to the molecular distribution in a solution, and according to the considerations done above on the suitability of ethanol, a solution containing CTAB and TPBI in ethanol, in the same stoichiometry of the sample, was prepared and measured. This solution gave Stokes shifts of 157 nm for the TPBI alcohol solution and 159 nm for the mix (CTAB + TPBI in ethanol) (see Table 2). Finally, the quantum yields (QY) of all samples were recorded with the "De Mello method"[37–39] and are reported in Table 2 as averages with their standard deviations. The QYs of all the solid samples are lower than the QY of TPBI in dichlorometane (59%) but they represent good results, ranging between 53 and 57%, especially when this value is coupled to a large Stokes shift, that is crucial for the application of the final material as light harvester for PV. In other words, a good compromise with acceptable Stokes shift and quantum yield was obtained.

Conclusions

A LAG procedure was implemented to obtain the intercalation of an organic neutral molecule into anionic lamellar matrices, and it has proved a facile, fast, and clean method to obtain efficiently nanocomposites by the cation exchange processes. This procedure reduced the time and the cost of the exchange, while reducing solvent waste with an improved environmental profile. In particular, the LAG method was exploited for the dispersion of a neutral molecule mediated by a cationic surfactant, CTAB. The dispersion of a neutral molecule occurs because the CTA^+ counterbalances the anionic charge of the saponite and the alkyl chains promote the delivery of the neutral species by means of Van der Waals interactions.

The *CTA_TPBI_Sap* was synthetized and characterized, showing good optical features (Stokes Shift larger than 100 nm and quantum yield above 50%) also in the photoactive polymer sample. Interestingly, the dispersion of this sample in the Kurarity co-polymer has improved the Stokes shift, as probably the extrusion promotes an efficient delamination of saponite, reducing the π–π interaction between the fluorophore molecules. Conversely, the quantum yield of the *Kur_CTA_TPBI_Sap* is about 4.5% lower than that of *CTA_TPBI_Sap* (58%) and about

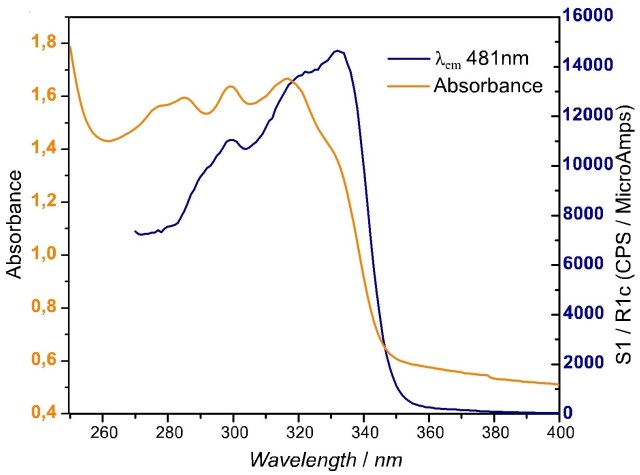

Figure 8. UV–Vis spectrum in transmission (orange) of *Kur_CTA_TPBI_Sap* film and fluorescence excitation spectrum at λ 481 nm (blue).

Table 2. Stokes Shifts and Quantum Yields (QYs).

Sample	Stokes Shift (nm)	Yield 1	Yield 2	Yield 3	Avg. (%)	Std.dev.
CTA_TPBI_Sap	108	57.58	56.64	58.06	57.43	0.72
Kur_TPBI	159	54.93	54.62	58.22	55.92	2.00
Kur_CTA_TPBI_Sap	161	51.44	53.54	53.64	52.87	1.25
TPBI[a]	159	64.55	64.62	64.12	64.43	0.27
TPBI CTAB[a]	157	62.08	63.67	63.48	63.08	0.87

[a] Ethanol solution.

11.5% lower than that of TPBI in ethanol. This decrease could be ascribed to the Kurarity matrix and the additive loadings, because also the quantum yield of the TPBI not intercalated (*Kur_TPBI*) is about 8.5% lower than that of TPBI in ethanol solvent and about 7% lower with respect to the TPBI in ethanol with CTAB.

Given the large use of clays as additive in polymers, ranging from epoxy resins, to PVC,[14,40] we can infer that this approach can be extended to other kind of polymers.

In conclusion, the intercalation of the dye with a surfactant proved to be an effective way of dispersion since the performances of the dye were almost as good as in ethanol solution and allow easy dispersion in the polymer in prospect of a scale-up to industrial application.

This work demonstrated the applicability of the LAG procedure for intercalation into cationic clays, providing new opportunities to obtain fully synthetic, host-guest functional materials. Moreover, the control of saponite synthesis can provide materials with other physical and chemical properties, by tailoring CEC and dimensions.

Experimental Section

Materials

Chemicals were purchased by Sigma Aldrich and used without further purification. TPBI dye was synthetized according to the procedure already reported in literature by Fahrni et. al..[28] Briefly, a solution of 2-(2′-aminophenyl)benzimidazole and *p*-toluenesulfonyl chloride in pyridine was stirred at room temperature for several hours. The mixture was poured into H_2O, neutralized with HCl, and extracted with ethyl acetate. The combined organic phase was washed with H_2O, dried with $MgSO_4$, filtered, concentrated in vacuo, and then purified by flash chromatography on silica gel.

The poly(methyl methacrylate)-block-poly(n-butyl acrylate) (PMMA-PnBA block co-polymer) Kurarity LA 4285 specifically designed for PV applications by Kuraray Co. (Japan) was chosen for the compounding tests, due to its high transparency and UV resistance.

NaSap110 was obtained through hydrothermal synthesis and purified to the sodic form, as already reported in the literature.[21]

Incorporation of CTAB and TPBI into NaSap110

The preparation of the sample was carried out adapting the liquid assisted grinding method that was tested with the intercalation of fluorene.[21] TPBI (0.1620 g) and CTAB (0.4538 g) in a ratio 0.35:1, were grinded in a zircon ball mill for 5 min at 20 rps with 3.00 mL of ethanol and then 0.6389 g of NaSap110 (CEC equal to 50.9 meq/100 g saponite, obtained by CoHex method[35]) and another 3.00 mL of ethanol were added inside the mill and grinded for another 5 minutes before drying in an oven at 50 °C for one hour. This dried sample, named CTA_TPBI_Sap was abundantly washed and filtered with water and ethanol to remove the excess of surfactant and neutral molecules.

XRPD analysis

X-ray powder diffraction measurements were performed on a ThermoARL powder diffractometer XTRA48 equipped with a solid state Peltier cooled detector using the Bragg Brentano geometry and Cu Kα radiation (λ = 1.54062 Å). All patterns were measured in continuous mode using the following conditions: 2θ angular range 2–70°; tube power 45 kV and 40 mA, step size 0.02°2θ, scan rate 0.5°/min.

SEM analysis

SEM images at different magnification were recorded on a Quanta 200 FEI Scanning Electron Microscope equipped with EDAX EDS attachment, using a tungsten filament as electron source at 25 KeV. For the morphological analysis a dispersion of the sample in ethanol was directly deposed on the hot stub. The dispersion was obtained after sonication in ethanol for 40 minutes of a small amount of grinded powder sample. The elemental composition of some samples prepared for morphological analysis were evaluated with the EDAX EDS apparatus. The samples were coated with an Au layer with a thickness range from 10–45 nm to improve the conductivity. Elemental mapping was performed on samples showing the presence of different morphologies. To avoid interferences from the aluminum stub and sulfur contained in the adhesive tape, a pellet of a PMMA-PnBA block co-polymer (Kurarity LA 4285),[20] was directly melt on the stub and a sample dispersion in ethanol was dripped on it. The sample was not metallized since the Mα emission of gold would be superimposed on the Kα emission of sulfur, influencing its determination. The SEM images and EDX on the polymer films were taken after washing with milliQ water. The films were cold cut with a hollow punch, fixed to the stub with adhesive tape and coated with 30 nm of carbon. Elemental maps on the image were collected with a dwell of 40 msec (time of stay) for a total collection time of 3 hours.

X-Ray Fluorescence Spectroscopy (XRF)

XRF analysis were carried out using a Rigaku NEX QC Benchtop Energy Dispersive X-ray Fluorescence (EDXRF) spectrometer, equipped with a 4 W X-ray tube. Helium purge flow was used. The calibration curve was obtained using three standards made of a mixture of saponite, CTAB and TPBI in three ratios covering the expected range for the sample. For the measure of Br the X-ray tube was set to 30 kV and 25 μA and collection time to 90 s. A filter to optimize performance by selectively reducing the scattering from the x-ray tube thus creating "quiet spots" in the background signal for the elements from Ca to Zr was used. Si, Mg, Al, and S were instead measured without filter and the tube was set to 6.5 kV and 100 μA and collection time to 300 s. To obtain Si, Mg and Al amounts a deconvolution of the signals was performed.

Elemental Analysis (EA)

The amount of carbon, nitrogen, hydrogen and sulfur was detected by using the EuroVector CHNS analyzer "EA3000". Reaction tube and GC oven temperatures were 980 °C and 100 °C, respectively. The helium flow was 80 mL min^{-1}. Oxygen (12 mL) was injected at 35 kPa. The run time was 400 s and the retention time of the gases were 33.0 s for N_2, 52.0 s for CO_2, 170.0 s for H_2O and 265.0 s for SO_2. Atropine sulphate was the standard for the instrument calibration. 0.5–1.5 mg of each sample was put into a tin capsule (3.5 × 5 mm) closed outgassed and analyzed.

Mass Spectrometry (MS)

Electrospray ionization mass spectra (ESI MS) were recorded on a SQD 3100 Mass Detector (Waters), operating in positive or negative ion mode, with 1% v/v HCOOH in methanol as the carrier solvent.

Spectroscopic characterization

Fourier Transformation Infrared Spectroscopy (FT-IR) analyses were performed on a Fourier transform infrared (FTIR) Nicolet 5700 spectrometer (Thermo Optics) at a resolution of 4 cm^{-1} in the spectral range from 4000 to 400 cm^{-1} and 128 scans. This instrument is equipped with transmission module and other apparatuses, as an Attenuated Transmission Reflectance (ATR) and a microscope bench. The powder samples were measured in transmission, after grinding in KBr pellet using a sample/KBr weight ratio of 1:100. The ATR measures were led on the polymeric films. Finally, the Microscope bench (featuring a liquid N_2 cooled MCT detector) was exploited for the mapping of polymeric films.

Raman Spectra were recorded on a Fourier-transformed Bruker RFS100 spectrophotometer, equipped with a Nd:YAG laser, emitting at 1.064 nm (NIR region), as the excitation source, and a liquid-nitrogen cooled Ge detector. Instrumental resolution was set at 4 cm^{-1} in the range of Raman shift 3500–200 cm^{-1} and number of scansions were selected in based of the sample signal.

Steady-state emission spectra were recorded on a Horiba Jobin_ Yvon Model IBH FL-322 Fluorolog 3 spectrometer implemented with a 450 W xenon arc lamp, double grating excitation and emission monochromators (2.1 nm/mm dispersion; 1200 grooves/mm), and a Hamamatsu Model R928 photomultiplier tube. Emission spectra were corrected by the standard correction curve.

Termogravimetric analysis

Thermogravimetric analysis (TGA) was performed on a Setaram SETSYS Evolution instrument under helium gas flow, with a gas flow of 20 mL/min. The samples were heated from 30 to 900 °C with a rate of 10 °C/min. Thermograms were corrected by subtraction of the background curve, obtained without sample in the same experimental conditions.

TGA-GC-MS hyphenated technique

TG-GC-MS hyphenated technique is a combination of a Thermogravimetric balance, a Gas-Chromatography Spectrometer for the separation, and a Mass Spectrometer instrument as detector. Thermogravimetric analysis under inert gas and TGA-GC-MS analysis were collected using a Mettler TGA/SDTA 851e working with Helium flow. Measures were performed from 25 to 700 °C with a heating rate of 10 °C/min using alumina crucibles. GC-MS section is based on a FINNIGAN TRACE GCULTRA and TRACE DSQ, equipped with a Phenomenex DB5-5 ms capillary column (30 m, 0.25 mm i.d., 0.25 mm thickness), in a thermostatic oven at 200 °C. The splitless injector was heated at 250 °C and chromatographic runs were carried on in helium (1.0 mL/min). and 200 °C, respectively. The collection of the evolved gas from TGA was performed with a custom-made interface. Two heated transfer lines at 250 °C, one (HTL1) from TGA to an automatic gas sampling system (AI) system (working at 200 °C), and a second one (HTL2) from the AI to the GC-MS injector port allow the delivery of the exhaust of TG to chromatographic separation. Sampling of exhaust gas was based on an injection loop of 2.5 mL and the sampling frequency was 30 s^{-1}. The transfer to MS was provided by a heated transfer line set at 270 °C. The MS signal was acquired in EI+ mode with ionization energy of 70.0 eV and at the ion source temperature of 250 °C. The acquisition was performed both in full-scan mode, in the 20–350 m/z range and in Single Ion Monitoring (SIM) mode by acquiring the signals corresponding to the main m/z peaks of given molecules. The identification of the evolved products was performed by comparison of the retention times and MS spectra of reference standards analyzed in the same experimental conditions.

The TGA stage was performed by heating at the same rate adopted in the previous measures (10 °C/min) under helium flow.

The mass spectrometric acquisitions were recorded both in full-scan mode, in the 20–350 m/z range and in Single Ion Monitoring (SIM) mode by acquiring the signals characterizing the CTAB (fragment at m/z = 58) and TPBI (fragment at m/z = 91). On the NaSap110, the scan of the same m/z fragments (58; 91) was performed, to obtain the matrix background. The identification of the evolved products was performed by comparing of the retention times and the TG-GC-MS spectra of the reactants measured in the same experimental conditions.

Compounding tests and filming

Compounding tests were performed by using a laboratory Thermo HAAKEÏ MiniLab II Micro Compounder. The system is based on a conical, twin-screw compounder with an integrated backflow channel. As a result of the channel and a bypass valve, the residence time can be finely controlled.

For the extrusion of *Kur_CTA_TPBI_Sap*, *Kur_NaSap110* and *Kur_TPBI* the temperature was set to 160 °C with a screw rate circulation equal to 125 cycles/min for 5 minutes.

The filming procedure exploited a Specac press equipped with heated metal plates and a set of rings to obtain the desired thickness. About 200 milligrams of chopped string were placed on the hot plate at 130 °C on a smooth aluminum foil inside a ring of 100 μm thickness and covered with another aluminum foil before pressing; this procedure allowed for obtaining uniform, 100 μm thick films.

Acknowledgements

We gratefully acknowledge Prof. M. Zanetti for his help and suggestions in performing compounding test. C. B, N. B., S. G. acknowledge support from the Project CH4.0 under the MUR program "Dipartimenti di Eccellenza 2023–2027" (CUP D13C22003520001).

Conflict of Interests

The authors declare no conflict of interest.

Data Availability Statement

The data that support the findings of this study are available in the supplementary material of this article.

Keywords: Clays · Green chemistry · Light management · Organic-inorganic hybrid composites · TGA-GC-MS

[1] E. Klampaftis, D. Ross, K. R. McIntosh, B. S. Richards, *Sol. Energy Mater. Sol. Cells* **2009**, *93*, 1182–1194.
[2] M. B. de la Mora, O. Amelines-Sarria, B. M. Monroy, C. D. Hernández-Pérez, J. E. Lugo, *Sol. Energy Mater. Sol. Cells* **2017**, *165*, 59–71.
[3] W. G. J. H. M. van Sark, K. W. Barnham, L. H. Slooff, A. J. Chatten, A. Büchtemann, A. Meyer, S. J. McCormack, R. Koole, D. J. Farrell, R. Bose, E. E. Bende, A. R. Burgers, T. Budel, J. Quilitz, M. Kennedy, T. Meyer, C. De Mello Donegá, A. Meijerink, D. Vanmaekelbergh, *Opt. Express, Vol. 16, Issue 26, pp. 21773–21792* **2008**, *16*, 21773–21792.
[4] S. Ueno, S. Fujihara, *J. Electrochem. Soc.* **2011**, *158*, K1.
[5] E. Conterosito, G. Croce, L. Palin, E. Boccaleri, W. van Beek, M. Milanesio, *CrystEngComm* **2012**, *14*, 4472.
[6] C. E. Housecroft, E. C. Constable, *Chem. Sci.* **2022**, *13*, 1225–1262.
[7] N. Yao, J. Huang, K. Fu, X. Deng, M. Ding, M. Shao, X. Xu, *Electrochim. Acta* **2015**, *154*, 273–277.
[8] G. Volpi, S. Galliano, R. Buscaino, G. Viscardi, C. Barolo, *J. Lumin.* **2022**, *242*, 118529.
[9] Z. Wang, A. Meijerink, *J. Phys. Chem. Lett.* **2018**, *9*, 1522–1526.
[10] R. Caliandro, V. Toson, L. Palin, E. Conterosito, M. Aceto, V. Gianotti, E. Boccaleri, E. Dooryhee, M. Milanesio, *Chem. A Eur. J.* **2019**, *25*, 11503–11511.
[11] R. Baby, P. D. Nixon, N. M. Kumar, M. S. P. Subathra, N. Ananthi, *Environ. Sci. Pollut. Res. Int.* **2022**, *29*, 371–404.
[12] G. Volpi, G. Magnano, I. Benesperi, D. Saccone, E. Priola, V. Gianotti, M. Milanesio, E. Conterosito, C. Barolo, G. Viscardi, *Dyes Pigm.* **2017**, *137*, 152–164.
[13] L. Etgar, J. Park, C. Barolo, V. Lesnyak, S. K. Panda, P. Quagliotto, S. G. Hickey, M. K. M. K. Nazeeruddin, A. Eychmüller, G. Viscardi, M. Grätzel, *RSC Adv.* **2012**, *2*, 2748–2752.
[14] S. Xue, T. J. Pinnavaia, *Microporous Mesoporous Mater.* **2008**, *107*, 134–140.
[15] Z. P. Xu, P. S. Braterman, in *Dekker Encyclopedia of Nanoscience and Nanotechnology*, (Eds.: J. A. Schwarz, S. . Lyshevski, C. I. Contescu), CRC Press., Boca Raton, **2008**, p. 1841–1852.
[16] E. N. Kalali, X. Wang, D.-Y. Wang, *J. Mater. Chem. A* **2016**, *4*, 2147–2157.
[17] E. N. Kalali, X. Wang, D.-Y. Wang, *J. Mater. Chem. A* **2015**, *3*, 6819–6826.
[18] Y. Gao, Y. Zhao, L. Qiu, Z. Guo, D. O'Hare, Q. Wang, *Polym. Compos.* **2015**, DOI: 10.1002/pc.23764.
[19] C. H. Zhou, Q. Zhou, Q. Q. Wu, S. Petit, X. C. Jiang, S. T. Xia, C. S. Li, W. H. Yu, *Appl. Clay Sci.* **2019**, *168*, 136–154.
[20] E. Conterosito, I. Benesperi, V. Toson, D. Saccone, N. Barbero, L. Palin, C. Barolo, V. Gianotti, M. Milanesio, *ChemSusChem* **2016**, *9*, 1279–1289.
[21] V. Toson, D. Antonioli, E. Boccaleri, M. Milanesio, V. Gianotti, E. Conterosito, *Molecules* **2022**, *27*, 3048.
[22] V. Toson, *PhD thesis*, Università del Piemonte Orientale (IT), **2018**.
[23] E. Conterosito, V. Gianotti, L. Palin, E. Boccaleri, D. Viterbo, M. Milanesio, *Inorg. Chim. Acta* **2018**, *470*, 36–50.
[24] L. A. Utracki, M. Sepehr, E. Boccaleri, *Polym. Adv. Technol.* **2007**, *18*, 1–37.
[25] J. T. Kloprogge, L. Hickey, R. L. Frost, *J. Mater. Sci. Lett.* **1999**, *18*, 1401–1403.
[26] K. H. Ong, B. Liu, *Molecules* **2017**, *22*, 897.
[27] C. Crevant, C. Lucchesi, M. Paire, J. F. Guillemoles, *Phys. Status Solidi C* **2017**, *14*, 1700178.
[28] C. J. Fahrni, M. M. Henary, D. G. VanDerveer, *J. Phys. Chem. A* **2002**, *106*, 7655–7663.
[29] D. Martin, M. Rouffet, S. M. Cohen, *Inorg. Chem.* **2010**, *49*, 10226–10228.
[30] M. Milanesio, E. Conterosito, D. Viterbo, L. Perioli, G. Croce, *Cryst. Growth Des.* **2010**, *10*, 4710–4712.
[31] V. Gianotti, D. Antonioli, K. Sparnacci, M. Laus, T. J. Giammaria, M. Ceresoli, F. Ferrarese Lupi, G. Seguini, M. Perego, *J. Chromatogr. A* **2014**, *1368*, 204–210.
[32] V. Gianotti, D. Antonioli, K. Sparnacci, M. Laus, C. Cassino, F. Marsano, G. Seguini, M. Perego, *J. Anal. Appl. Pyrolysis* **2017**, *128*, 238–245.
[33] E. Conterosito, L. Palin, D. Antonioli, D. Viterbo, E. Mugnaioli, U. Kolb, L. Perioli, M. Milanesio, V. Gianotti, *Chem. A Eur. J.* **2015**, *21*, 14975–14986.
[34] C. Bisio, G. Gatti, E. Boccaleri, L. Marchese, G. B. Superti, H. O. Pastore, M. Thommes, *Microporous Mesoporous Mater.* **2008**, *107*, 90–101.
[35] H. Ciesielski, T. Sterckeman, M. Santerne, J. P. Willery, *Agron. Agric. Environ.* **1997**, *17*, 1–7.
[36] F. Thomas, L. J. Michot, D. Vantelon, E. Montargès, B. Prélot, M. Cruchaudet, J. F. Delon, *Colloids Surf. A* **1999**, *159*, 351–358.
[37] G. Accorsi, G. Verri, M. Bolognesi, N. Armaroli, C. Clementi, C. Miliani, A. Romani, *Chem. Commun.* **2009**, *23*, 3392– 3394.
[38] L. Porres, A. Holland, L. Pålsson, A. Monkman, C. Kemp, A. Beeby, *J. Fluoresc.* **2006**, *16*, 267–273.
[39] N. P. D. O. Faulkner, J. J. McDowell, A. J. Price, D. D. Perovic, K. Ozin, G. Ozin, *Laser Photon. Rev.* **2012**, *6*, 802–806.
[40] C. H. Zhou, Q. Zhou, Q. Q. Wu, S. Petit, X. C. Jiang, S. T. Xia, C. S. Li, W. H. Yu, *Appl. Clay Sci.* **2019**, *168*, 136–154.

Manuscript received: June 8, 2023
Revised manuscript received: June 13, 2023
Accepted manuscript online: June 14, 2023
Version of record online: July 3, 2023